Carbohydrate Polymers 291 (2022) 119541

Contents lists available at ScienceDirect

Carbohydrate Polymers

journal homepage: www.elsevier.com/locate/carbpol

Three methods to measure the dissolution activation energy of cellulosic fibres using time-temperature superposition

Yunhao Liang, Michael E. Ries *, Peter J. Hine

School of Physics and Astronomy, University of Leeds, Woodhouse Lane, Leeds LS2 9JT, UK

ARTICLE INFO

Keywords:
Cellulose
Ionic liquid
Time-temperature superposition
Hydrogel
Dissolution activation energy

ABSTRACT

Three methods are established to explore the dissolution kinetics of cellulosic fibres in the ionic liquid 1-ethyl-3-methyl-imidazolium acetate ([C2mim][OAc]), based on optical microscopic images of processed dried cellulose and cellulose hydrogels. The dissolution process for different times at various temperatures was analysed using time-temperature superposition, and from this the dissolution was found to follow an Arrhenius behaviour. Three values for the activation energy of dissolution were obtained from three different quantifying methods; these were found to agree, giving an average value of 73 ± 2 kJ/mol. A new method is developed to determine the swelling ratio of different regions of the processed cellulose samples, along with the different water volume fractions contained therein. The findings will be of interest to researchers making all cellulose composites and those studying the dissolution of cellulose by ionic liquids.

1. Introduction

Cellulose is a semi-crystalline polysaccharide and the most abundant biomaterial on earth, offering a green alternative to the fossil fuel based synthesized polymers (Lynd et al., 2002). Due to its specific physical and chemical properties, i.e. the abundant intra and intermolecular hydrogen bonds which act as crosslink points, the degradation temperature is lower than its melting point, which makes it difficult to melt without any chemical modifications (Quintana et al., 2012). In addition to the hydrogen bond network there are hydrophobic interactions between the anhydroglucose ring units, making cellulose insoluble in water and most common organic solvents (Glasser et al., 2012; Lindman et al., 2010).

Cellulose can only be dissolved by breaking down the hydrogen bond network, either with or without prior chemical modification (Sen et al., 2013). Most of the chemical modification processes are environmentally harmful, such as the use of carbon disulphide, aqueous sodium hydroxide and sulphuric acid, with H_2S produced during the Viscose process. *N*-methylmorpholine-N-oxide monohydrate (NMMO) (Zhao et al., 2007), Lithium Chloride/*N*, *N*-Dimethylacetamide (LiCl/DMAc) (McCormick et al., 1985; Zhang et al., 2012), sodium hydroxide (NaOH) aqueous solution (Isogai & Atalla, 1998) have been found to dissolve cellulose directly without the need of chemical modification. However, there are a number of drawbacks in their application on dissolving cellulose, such as a high energy cost (below 0 °C or much higher than room temperature for dissolution), low stability of solutions (NMMO/water systems) and low maximum cellulose concentration (LiCl/DMAc systems). For example, a low temperature (around −5 °C) is usually needed for NaOH aqueous solution to dissolve cellulose with a maximum concentration of about 8 wt% cellulose (Budtova & Navard, 2016).

Ionic liquids (ILs) are entirely composed of ions, cations and anions, which are in the liquid state below 100 °C (Plechkova & Seddon, 2008; Walden, 1914). Due to their high thermostability, extremely low vapor pressure, potential recyclability and tunable properties (Mahmood et al., 2017), they are candidates for 'green' solvents for cellulose dissolution. Even though ionic liquids have been reported since 1914 (Walden, 1914), after the pioneering studies on cellulose dissolution in dialkylimidazolium-based ILs, (Swatloski et al., 2002) they have more recently started to draw significant attention as cellulose solvents (Chen et al., 2020; Cuissinat et al., 2008b; El Seoud et al., 2007; Ries et al., 2014). For coagulating the cellulose from its solution, coagulation agents such as water and ethanol are often used to remove the ILs (Cao et al., 2014). A drying process is then followed to evaporate the coagulation agents. The water content in cellulose based hydrogels plays an important role in the physio-mechanical properties and their functioned properties as smart materials (Chang et al., 2010; Kabir et al., 2018), and this is usually measured according to the weight loss before and after a

* Corresponding author.
E-mail addresses: pyyl@leeds.ac.uk (Y. Liang), m.e.ries@leeds.ac.uk (M.E. Ries), p.j.hine@leeds.ac.uk (P.J. Hine).

https://doi.org/10.1016/j.carbpol.2022.119541
Received 21 February 2022; Received in revised form 8 April 2022; Accepted 24 April 2022
Available online 28 April 2022

drying process (Saito et al., 2003).

Although applications of ILs on dissolution of cellulose have been reported for decades, its mechanism in this process is not yet fully understood. Some fundamental research has been reported on the kinetics and rheology of the dissolution of cellulose in ILs (Budtova & Navard, 2015; Chen et al., 2020; Gericke et al., 2009), where rheological activation energies (E_a) of cellulose/ILs solution are recorded to vary from 46 kJ/mol to 70 kJ/mol, depending on the IL and cellulose concentration. Recently, several published papers, including by these authors, show that the dissolution of cellulose in ILs follows an Arrhenius behaviour (Chen et al., 2020;Hawkins et al., 2021 ; Liang et al., 2021). Among these studies, the activation energy (E_a) of dissolution of 'natural/unprocessed' cotton and flax cellulose in [C2mim][OAc] were found to be 96 ± 3 kJ/mol and 98 ± 2 kJ/mol, respectively (Hawkins et al., 2021; Liang et al., 2021). But there has not been research found on 'processed/mercerized' cellulose using the method introduced in these two papers. In the pioneering work by Cuissinat et al. (Cuissinat et al., 2008a, 2008b; Cuissinat & Navard, 2006a, 2006b; Cuissinat & Navard, 2008) the dissolution of cellulose from different plants and some cellulose derivatives in NMMO, NaOH/additives (urea, ZnO, NMMO) aqueous system and ionic liquids were explored, among which there are four possible phases reported during the dissolution of cotton and wood fibres in 1-N-butyl-3-methylimidazolium chloride: phase 1, cellulose balloon formation; phase 2, cellulose balloon breaking; phase 3, dissolving the unswollen regions; phase 4, dissolving the cellulose balloon residues. This is widely accepted as the microscopic cellulose dissolving process with ionic liquids.

In this current study, the dissolution behaviour of a mercerized cotton – based cellulose in the ionic liquid, [C2mim][OAc], is investigated, upon processing with different combinations of temperature and time. The mercerization process is usually conducted on natural cotton with alkali aqueous solution to increase the adhesion of dyestuffs of cotton products, resulting in a lower cellulose molecular weight, less lignin and hemicelluloses, and a conversion from cellulose I to cellulose II (Yue et al., 2012). The partially dissolved cellulose is coagulated with the anti-solvent - water, forming a cellulose network filled and swollen by water in the pores, for the sake of simplicity, called hydrogels, then followed by a drying process. Optical microscopy (OM) is used to characterize the changes in morphology caused by different processing temperatures and/or times. The dissolution progress is quantified on both hydrogels and their dried samples, with different quantifying methods based on the results from OM. It is hypothesized that any parameters able to be tracked as a function of time and temperature can be used to check if time-temperature-superposition (TTS) holds, and the dissolution E_a is independent of quantifying method. Meanwhile, a novel and straightforward technique to measure the water content (volume fraction) in hydrogels is also presented and compared to the commonly used gravimetric method (Saito et al., 2003). The findings in this research can deliver informative knowledge and new methods for investigating other cellulose based/yarn materials and in the fabrication of all cellulose composites.

2. Experimental

2.1. Materials

The cellulose source used in this work was a mercerized cotton yarn (100 m-nr50, No. 1716, Coats Group plc, UK). 1-ethyl-3-methylimidazolium acetate ([C2mim][OAc]) with purity ≥95% was purchased from Sigma-Aldrich Corporation. The water content of [C2mim][OAc] was always below 0.5 wt% in the experiments, determined by a Karl Fischer titration machine (899 Coulometer, Metrohm U.K. Ltd., UK). A cold curing epoxy resin (Epoxicure, Cold Cure Mounting Resin from Buehler, UK) was used to embed samples for optical microscopy (OM) and Raman spectroscopy. Some essential information such as molecular weight and composition of the cellulose sample can be found in Tables S1 and S2.

2.2. Preparation methods

The dissolution process is quite similar to the one reported in our previous paper (Liang et al., 2021) and for completeness it is here described. The cotton yarns were wound on a Teflon frame where there were five single yarns separate from each other and an array with around 30 turns of yarns (for the wide-angle X-ray diffraction (WAXD) measurements), see Fig. S1. Then the samples with the frame were submerged in an excess [C2mim][OAc] bath (Le et al., 2014), with a solid to liquid mass ratio of ca. 1 to 40, contained in a Teflon dish. The [C2mim][OAc] bath had been preheated in a vacuum oven (Shellab 17 L Digital Vacuum Oven SQ-15VAC-16, Sheldon Manufacturing, Inc., USA) at the target temperature for 1 h. After being exposed for a certain period (0.25, 0.5, 1, 1.5, 2, 2.5, 3 and 4 h) at the target temperature, the samples were then taken out from the [C2mim][OAc] bath with special care to avoid any disturbance and put into a water bath to coagulate the dissolved cellulose. It should be noted that we are making the assumption that there was no significant cellulose loss in this step. The reproducibility of our results suggests that this is correct. This process was carried out under slowly running water for 24 h to remove [C2mim][OAc] thoroughly. It is noteworthy that a raw cotton yarn was also submerged in a water bath for 24 h as a control before observation, henceforward called 'the damp raw cotton yarn'. Thereafter, the resulting partially dissolved cellulose hydrogels, kept on the frames, were submerged in a water bath for OM and shown in Fig. S2, followed by a drying process at 120 °C for 1 h under vacuum during which the samples were kept on the frame to keep the length constant upon the drying process. Samples including hydrogels and dried partially dissolved single yarns for microscopy, and arrays with width above the diameter of the X-ray spot of 2 mm for WAXD were obtained.

Samples are named as CH-x-y and DCY-x-y, which represent a cellulose hydrogel (CH) and a dried cellulose yarn (DCY), prepared at temperature 'x' (°C) for 'y' hours.

2.3. Characterization and qualification

2.3.1. Optical microscopy

An optical microscope (BH2-UMA, Olympus Corporation, Japan) was used in transmission and reflection mode to explore the morphology of the CH (transverse view) and DCY (cross section), respectively. When being measured, the hydrogels were kept submerged in a water bath, after which they were dried and, each set of three DCY was embedded in an epoxy resin and polished down to the surface in order to allow the morphology of cross section to be investigated. The image processing software 'ImageJ 1.52d' was used for further size measurement with the assistance of its "Find Edges" function.

2.3.2. Water volume fraction and swelling ratio of cellulose hydrogels

The diameter of the sample is around 160 μm, causing a high difficulty to control the dryness commonly used in the gravimetric method. Therefore, a novel method to quantify the water content - the volume fraction- is introduced.

Fig. 1 (a) and (b) show typical images of transverse view of CH and cross section of DCY samples, respectively. It can be seen in both images that upon dissolution, the undissolved cellulose/central core is surrounded by an outer ring, which is the dissolved and subsequently coagulated fraction.

The changes in radial length of the outer ring and central core, labelled with red double-arrow lines and orange-arrow lines respectively in Fig. 1, are used to calculate the swelling ratio of the outer ring (R_{ring}) and central core (R_{core}):

$$R_{ring} = (a_H - b_H)/(a_D - b_D) \quad (1)$$

$$R_{core} = b_H/b_D \quad (2)$$

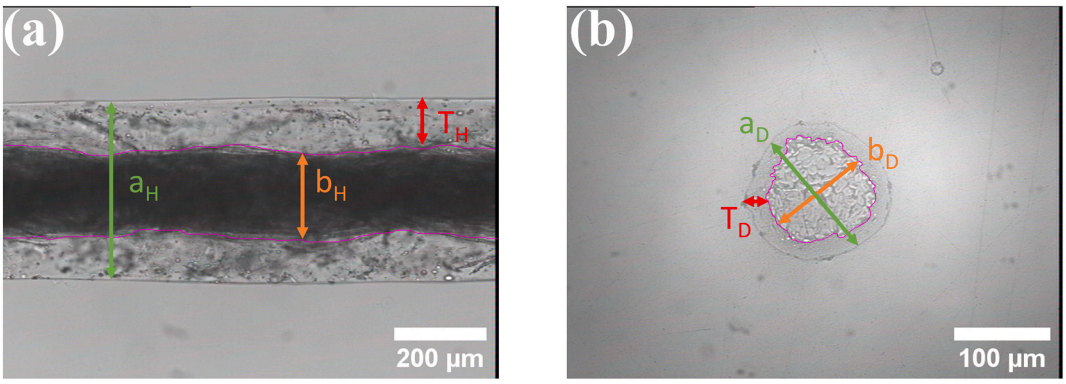

Fig. 1. (a) Transverse view of a cellulose hydrogel submerged in a water bath and (b) the cross section of the dried processed cellulose yarn obtained from an optical microscope, in which the undissolved section, the total sample and the outer ring are indicated in orange (b_H and b_D), green (a_H and a_D) and red (T_H and T_D) double-arrow lines, respectively; and the edges of the undissolved section for size measurement are outlined with purple lines in both images.

where a_H and b_H represent the outer diameter of the whole CH sample and the diameter of the central core of CH sample, respectively; while a_D and b_D measure the diameter of the whole DCY sample and that of the undissolved/central region of DCY respectively, recall Fig. 1. As to the size measurement of CH, three fibres were used, and 15 sampling points along the length of each fibre were applied, in order to calculate the means and standard errors of a_H and b_H.The outer ring thickness of the CH sample in water (T_H) and the DCY sample (T_D), were calculated by:

$$T_H = (a_H - b_H)/2 \tag{3}$$

$$T_D = (a_D - b_D)/2 \tag{4}$$

The water volume fraction, ϕ_{water}, of the different regions of the CH can also be calculated based on their micrographs via the equation below

$$\phi_{water} = \left(V_{swollen} - V_{dry}\right)/V_{swollen} \tag{5}$$

where $V_{swollen} = A_{swollen} \times L_{swollen}$ and $V_{dry} = A_{dry} \times L_{dry}$ represent the hydrogel volume and dried samples volume, respectively, and $L_{swollen}$ and L_{dry} means the length of hydrogels which are equal to each other. It is important to note that this is the upper limit of water fraction as the dried samples could contain cavities increasing V_{dry}. The equation above is rearranged to be:

$$\phi_{water} = \left(A_{swollen} - A_{dry}\right)/A_{swollen} \tag{6}$$

where $A_{swollen}$ and A_{dry} refer to the cross-section area of the hydrogel and the cross-section area of the dried samples; ϕ_{water}^{ring} and ϕ_{water}^{core} are used later to represent the water volume fraction in the outer ring and central core in the CH samples, respectively.

2.3.3. Quantification of dissolution

Three quantifying methods were applied in this study to quantify the dissolution process with various combinations of time and temperature. A coagulation fraction, CF_{DCY}, for the DCY is defined as:

$$CF_{DCY} = (A_{total} - A_{core})/A_{total} \tag{7}$$

where A_{total} and A_{core} measure the total cross-section area of DCY and the cross-section area of its central core. And for CH samples, the coagulation fraction, CF_{CH}, is calculated as:

$$CF_{CH} = \left[\pi(0.5a_H)^2 - \pi(0.5b_H)^2\right]/\left[\pi(0.5a_H)^2\right] \tag{8}$$

Besides, the ring thickness, T_H, of the CH samples is calculated via Eq. (3) and used as a parameter for dissolution quantification.

The growth of the three parameters, CF_{DCY}, CF_{CH} and T_H, with different processing times and temperatures is examined and analysed with TTS.

3. Results and discussion

3.1. Micromorphology

The processed cellulose yarns including both the cellulose hydrogels submerged in a water bath, and the dried cellulose yarns embedded in epoxy resins, were observed with an optical microscope, see Fig. 2.

As shown in Fig. 2(b)-(f) there are outer rings in CH samples, presenting in a lighter colour and covering the black central core, and they grew as the time/temperature increased. As is known in the literature (Chen et al., 2020; Cuissinat et al., 2008b; Liang et al., 2021), the dissolution starts from the exterior, and the outer rings are the dissolved and coagulated cellulose, which can be further verified by Raman spectroscopy, see Fig. S5, where a decrease in height of peaks at 379 cm^{-1}, 437 cm^{-1}, 520 cm^{-1} and 1476 cm^{-1} attributing to crystalline structure was found in the ring area, compared with the central region. The outer ring can also be seen in the micrographs of the dried samples, see Fig. 2(i)-(l). Moreover, the raw yarn consists of a bunch of filaments and each filament has a diameter of ca. 8.3 μm which as an assembly were swollen by the epoxy resin going between them, see Fig. 2(g). Thus, the diameter directly measured from Fig. 2(g) is not the correct value for the "raw sample" and alternative methods are used; this is discussed in more detail later.

For both DCY and CH samples, more coagulated cellulosic material was formed at higher dissolving temperatures and/or longer times. According to the micrographs, there was no coagulated cellulose observed in the central core, which is further confirmed by the Raman spectroscopy measurement, see Fig. S5. Compared with DCY, in CH samples the higher swelling ratio of the dissolved and coagulated cellulose amplifies the size of the outer ring of this component, allowing the growth to be followed more accurately with different processing temperatures and times.

3.2. Regional water volume fraction and swelling ratio in the radial-direction

The swelling ratio and water volume fraction of different regions upon the drying process was calculated by Eqs. (1), (2) and (6), according to the images shown in Fig. 3. For the swelling ratio and water volume fraction of the raw material, the picture of the dry raw yarn (Fig. 2(g)) cannot be used, as mentioned above, the filaments were separated due to the swelling effect of epoxy resin which leads to the sample appearing larger than the raw sample before being placed in the epoxy. Therefore, the sample processed at 30 °C for 0.25 h shown in Fig. 2(h) was used instead, which was processed at relatively low temperature and short time to avoid the filament separation found in raw samples, and gives the best measure of the 'dried' yarn cross section; this

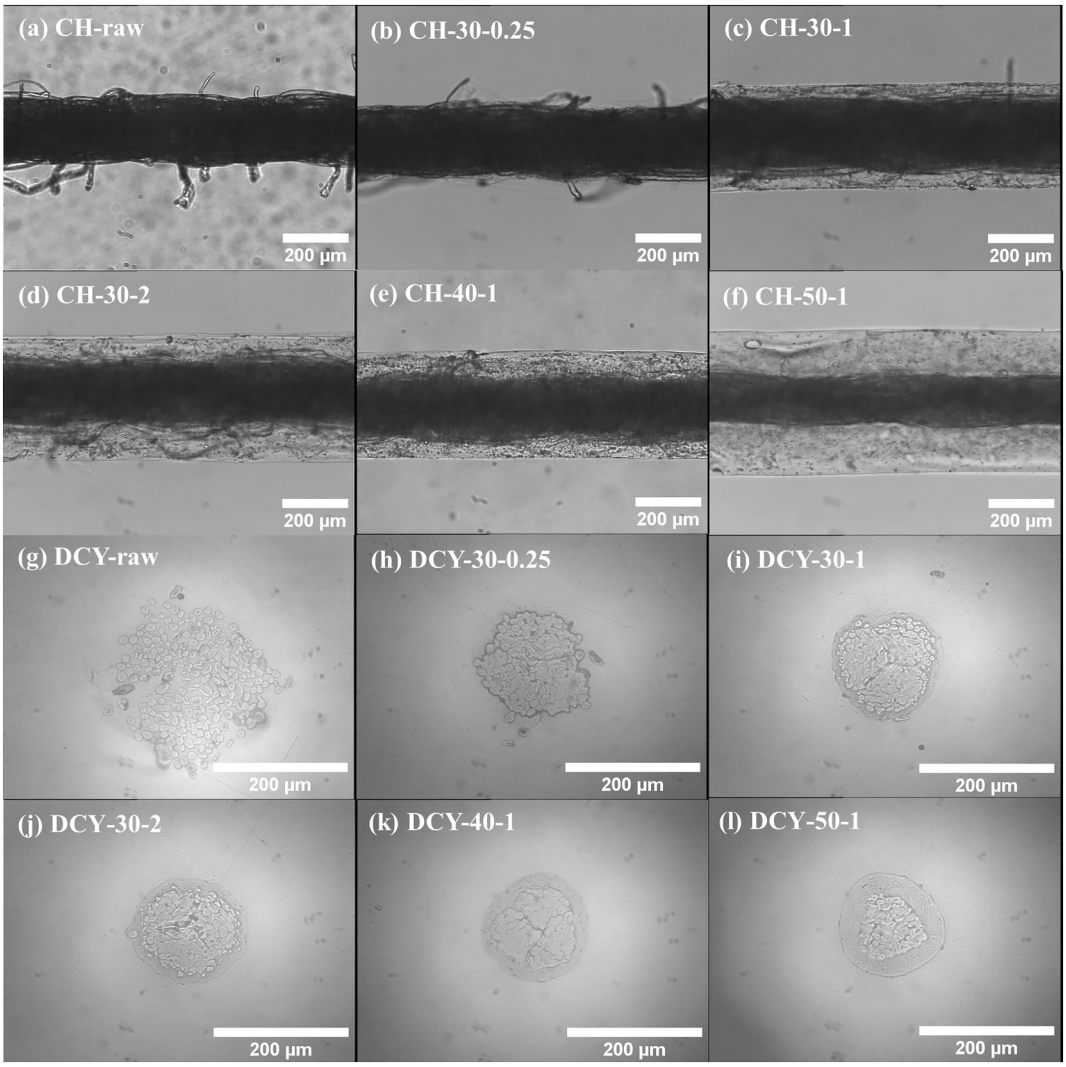

Fig. 2. Optical-microscopic transverse-view images of (a) the raw cotton yarn after soaking in water for 24 h and (b)-(f) the cellulose hydrogels (CH); cross-section images of (g) the raw cotton yarn and (h)-(l) the dried cellulose yarn (DCY) and look to section 2.2 for nomenclature in detail.

is subsequently further confirmed.

As shown from Fig. 3(a) and (b), the swelling ratio of both the outer ring and the central core is constant within the measurement uncertainties and is therefore independent of the dissolution time and temperature. The average swelling ratios of the outer ring and central core were found to be 5.0 ± 0.1 and 1.49 ± 0.05 respectively ($R \geq 1$, where 1 means that no change in size has occurred), which shows the outer ring swelled by ×3.4 as much as the central region.

Fig. 3 (c) and (d) indicate that the water volume fraction of either the outer ring or the central core also shows independence of the dissolving time and temperature. And it is 0.89 ± 0.01 in the outer ring which is about 1.6 times higher than that in the central core at 0.54 ± 0.02.

The water volume fraction of the damp raw sample (CH-raw in Fig. 2 (a)) is found to be 0.57 ± 0.02 which is very similar to that of central core in CH samples, 0.54 ± 0.02, and the same comparable results can be found in terms of swelling ratio. But those two properties of the damp raw sample are very different from those of the outer ring in CH samples. And as for the outer ring/coagulated region, there is more water filling the pores of cellulose molecular network after dissolution, leading to a higher water volume fraction and a subsequent larger swelling ratio than the central region. This implies that there was no or little coagulated cellulose in the central core. Therefore, the assumption that there is no dissolved/coagulated cellulose in the central region is confirmed. This also confirms the hypothesis that the dissolution proceeds from the exterior inwards and that the dissolved cellulose acts as a protective barrier for the inner cellulose.

To further explore the cellulose dissolution behaviour and to verify if CH-30-0.25 could correctly represent the dry raw sample when measuring the size, an approach to measure the theoretical values is introduced by plotting the radius of central core against the ring thickness to test the theoretical radii of both the DCY and CH samples, see Fig. 4.

The results show that as the ring thickness increases the size of central core decreases, and it follows a linear relationship independent of the temperature the measurements were carried out, strongly indicating that time-temperature equivalence is in operation. From Fig. 4, by extrapolating the ring thickness to zero on both lines – correspond to the raw material without any dissolution, giving both the theoretical radii for the DCY-raw and CH-raw to be 81 ± 2 μm and 124 ± 4 μm respectively. Therefore, a theoretical swelling ratio of raw material upon the drying process is calculated to be 1.53 ± 0.06, shown in Table 1. Compared with the results measured directly from the optical microscope pictures, the way of measuring the size of cotton yarns introduced in Fig. 4 is reliable due to their excellent agreement with each other, suggesting that in terms of size measurement, the DCY-30-0.25 approximately represents the dry raw material.

The method of measuring the water volume fraction used in this study makes the results more reliable than the usual gravimetric

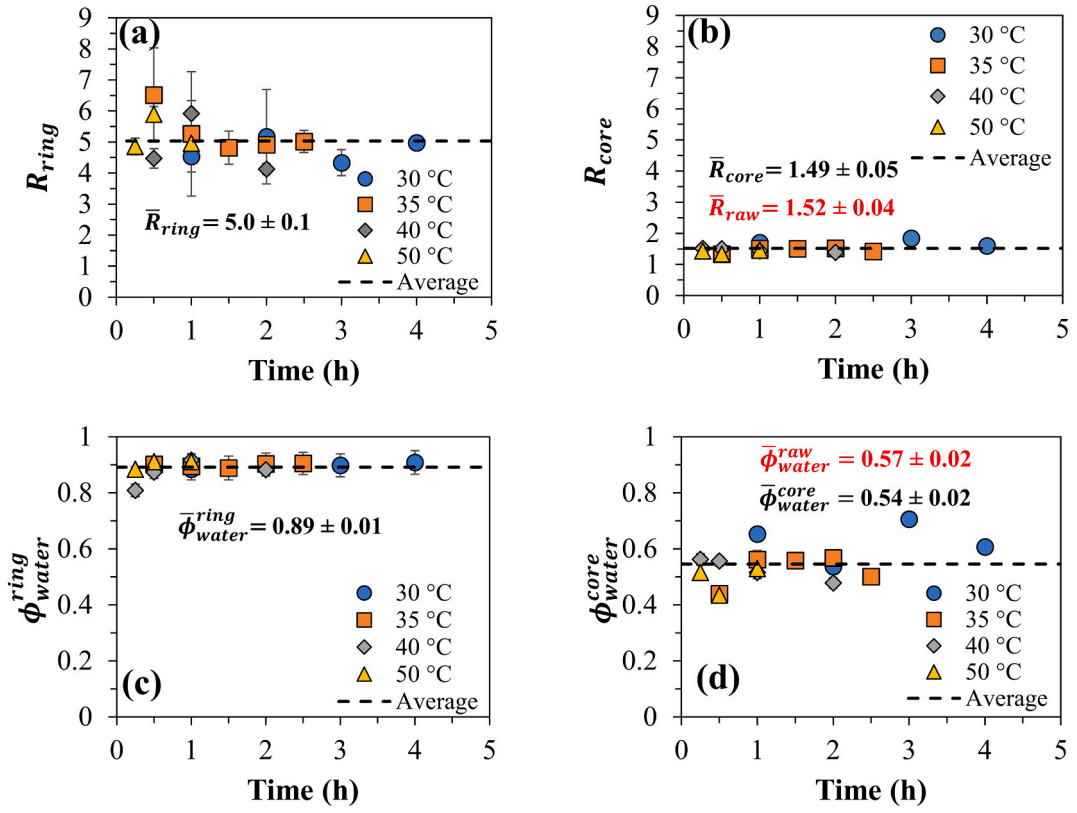

Fig. 3. Radial swelling ratio as a function of dissolution time for (a) the outer ring (R_{ring}) and (b) the central core (R_{core}) of cellulose hydrogels (CH) upon the drying process; and water volume fraction as a function of dissolution time of (c) the outer ring (φ^{ring}_{wate}) and (d) the central core (φ^{core}_{water}) of CH samples where the dash lines indicate the locations of the average values.

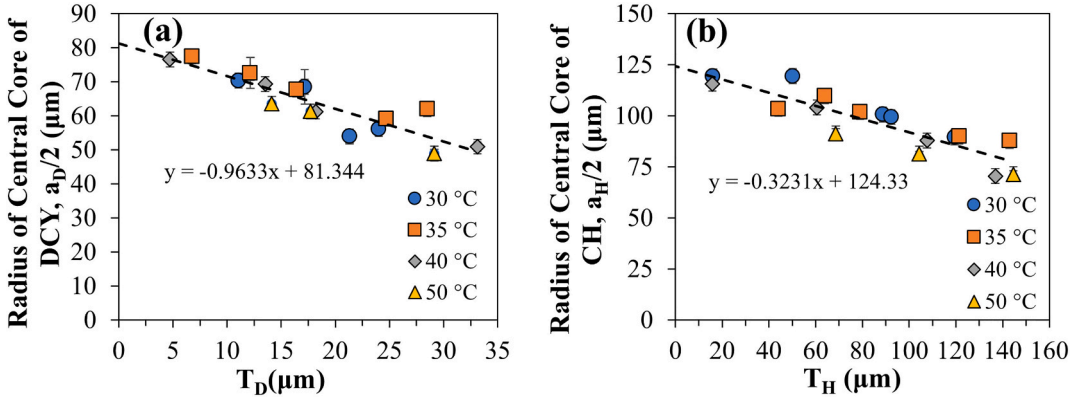

Fig. 4. The radius of the central core ($a_D/2$ and $a_H/2$) and the dependence of the ring thickness (T_D and T_H) in (a) dried samples and (b) hydrogels.

Table 1
the size of raw material at dry and damp status obtained from the extrapolation method and those in brackets measured directly from microscope pictures.

The radius of CH-raw in water (r′)/μm	The radius of DCY-raw (r)/μm	Swelling ratio (R_{raw} = r/r′)
124 ± 4 (122 ± 1)	81 ± 2 (80 ± 2*)	1.53 ± 0.06 (1.52 ± 0.04)

* The radius of dry raw yarn shown within the brackets was measured on the sample of DCY-30-0.25 by OM.

method. This is because during these measurements the hydrogels were kept submerged under water so that the influence of water evaporating, which would affect the results, is removed; this is especially the case for thin hydrogels of which the water evaporation will be faster, due to the higher specific surface area.

3.3. Understanding the dissolution of cellulose in [C2mim][OAc] by using TTS

3.3.1. The dried samples

The coagulation fraction of the DCY samples is calculated from Eq. (7) and the results are depicted in Fig. 5.

Fig. 5(a) shows that the coagulation fraction increases with both the processing time and temperature, which is in line with the qualitative results of the optical microscopy shown in Fig. 2. This agrees with the WAXD results in Fig. S3 and S4, where a conversion from cellulose I to cellulose II and amorphous cellulose was found upon processing and

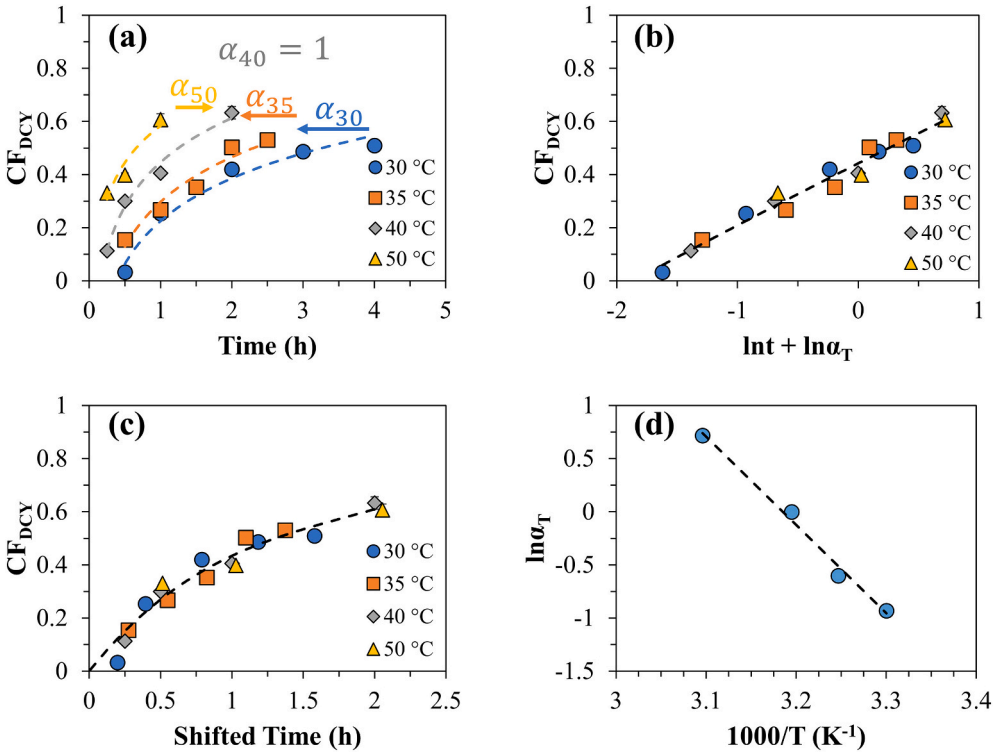

Fig. 5. (a) Coagulation fraction of DCY samples dependence of dissolving time and the time-temperature superposition plot after being shifted to 40 °C on both (b) natural-logarithmic time scale and (c) linear time scale; (d) Arrhenius plot with $R^2 > 0.99$; the dash lines in (a) and (c) are guide for the eye, and those in (b) and (d) are second-degree polynomial and linear fitting lines, respectively.

increased with dissolution proceeding, which is proved by a shifting from the peak at 22.4° (cellulose I) to the main cellulose II peak at 20.2°; and a decline in the ratio of peak 22.4° to the broad amorphous peak centred at 18.2°. A time-temperature equivalence is shown from the curves and a master curve was obtained at 40 °C. Shift factors were used to do the shifting at each temperature, T, to form the master curve, and the shifted dissolution time ($t_T^{'}$) can be obtained by the calculation with shift factor (α_T) and dissolution time (t_T) via:

$$t_T^{'} = t_T \times \alpha_T \tag{9}$$

and its natural logarithmic format is:

$$ln\left(t_T^{'}\right) = ln(t_T) + ln(\alpha_T) \tag{10}$$

The master curve at 40 °C was obtained as follows: The data points of 40 °C were chosen to be the reference set with a shift factor, α_{40}, to therefore be unity, i.e., all their dissolution times will be unchanged as they are multiplied by one, recall Eq. (9). For easier controlling the shift process, the linear time scale was converted to be a natural logarithmic time scale, $ln(t)$, as it now consists of a horizontal shift only, and the 40 °C data was fitted with a second-degree polynomial function for a visual guide for shifting the other temperature sets to. Thereafter, the other independent temperature set was horizontally shifted by a number, $ln\alpha_T$, to the reference set by eye. After this, a final second-degree polynomial function (the dash line in Fig. 5(b)) was used to fit all data sets, and finally, the shift factors at the other temperatures (α_{30}, α_{35} and α_{50}) were adjusted to maximize the R^2 value of all the data with respect to the final polynomial function, see Fig. 5(b). The order of the two polynomial functions were kept at the minimum required to adequately follow the data. This procedure is explained in more detail in our earlier work (Hawkins et al., 2021; Liang et al., 2021; Zhang et al., 2021).

The finalized master curves at 40 °C in natural logarithmic time and linear time scales are shown in Fig. 5(b) and (c), respectively. The formation of the master curves confirms the proposed time-temperature equivalence. Fig. 5(c) indicates the rate of dissolution decreased with time, one possible suggestion is that the dissolved cellulose acted as a protective barrier between the central region and the external solvent, and the larger dissolved region has higher protective effect.

A linear relationship between the $ln\alpha_T$ and the inverse temperature was found and plotted in Fig. 5(d), indicating the dissolution obeys an Arrhenius behaviour. An E_a of 69 ± 5 kJ/mol for this process was then calculated by Arrhenius equation:

$$ln\alpha_T = A - E_a/RT \tag{11}$$

where A, E_a, R and T are the Arrhenius pre-factor, activation energy, gas constant and temperature in kelvin, respectively. The uncertainty is calculated by a linear regression optimisation in Excel (LINEST).

3.3.2. *The hydrogels*

Two other methods to follow the growth of the coagulation fraction and the ring thickness based on the submerged (CH) samples were investigated. This does not require the drying, encapsulation and the polishing process and therefore saves significant time in investigating dissolution behaviour. According to the Eq. (3) and (8), T_H and CF_{CH} were calculated, and their dependences of dissolving time are shown in Fig. 6.

Shown in Fig. 6(a) and (d), both the CF_{CH} and T_H increased with time and/or temperature increasing, which is consistent with how the CF_{DCY} changed with time and temperature (Fig. 5). Time-temperature equivalence was again used to construct master curves at 40 °C using the same process as described above in Fig. 5. TTS analysis was applied for each quantifying method according to the same routine as above. A linear relationship between $ln\alpha_T$ and the inverse of temperature was again found for both measures of the dissolution and plotted, see Fig. 6(c) and (f), giving E_a of 78 ± 4 kJ/mol and 71 ± 4 kJ/mol from measuring the CF_{CH} and T_H of the hydrogels respectively. This is in excellent agreement with the value of 69 ± 5 kJ/mol obtained from the analysis of the dry

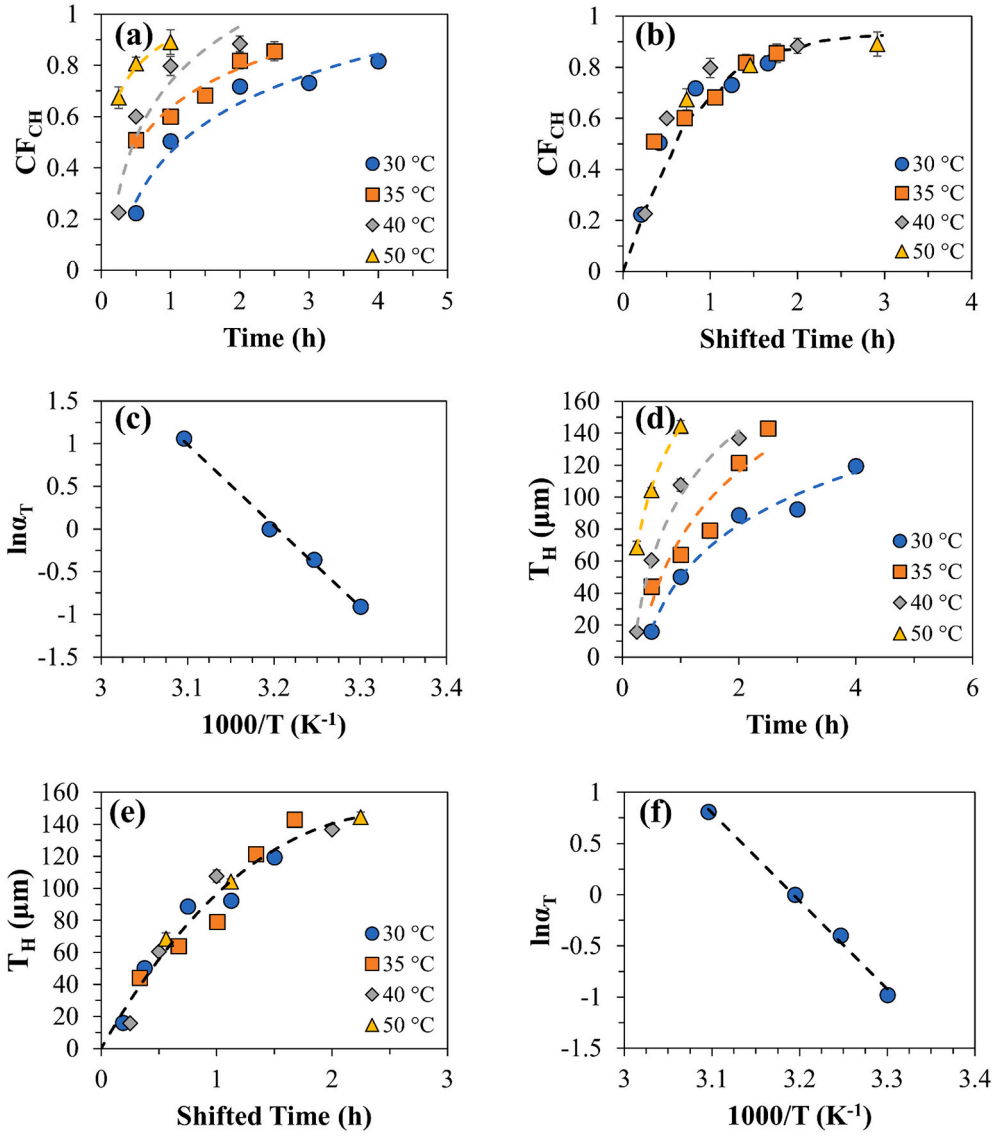

Fig. 6. (a) Coagulation fraction,CF_{CH}, based on microscopy results of hydrogels, as a function of dissolving time, (b) its master curve and (c) Arrhenius plot with $R^2 > 0.99$; (d) ring thickness, T_H, based on microscopy results of hydrogels, dependence of dissolving time, (e) its master curve and (f) Arrhenius plot with $R^2 > 0.99$; the dash lines in (a), (b), (d) and (e) are guide for the eye, and those in (c) and (f) are linear fitting lines.

(DCY) samples. This indicates that all the three quantities can effectively measure the dissolution process where the hydrogen bonds among cellulose molecules are broken by [C2mim][OAc], consequently leading to the measurable change in those quantities as a result of molecule/ion diffusion which is controlled by time and temperature; and the measurement of the hydrogels is an excellent methodology for following the dissolution of cellulose fibres and determining the activation energy E_a, as it does not require encapsulation and the drying process. Additionally, the outer ring in CH samples is much easier to distinguish for lower processing temperatures and times.

3.4. Comparison of different methods of analysing the dissolution of cellulose in [C2mim][OAc]

The E_a obtained from three different methods are summarized in Table 2.

The activation energies in Table 2 show an independence of the quantifying parameter, giving an average value of 73 ± 2 kJ/mol. This result on the mercerized cotton confirms universality of the TTS method reported in the paper (Liang et al., 2021) on a natural cotton.

Table 2
Comparison of activation energies obtained from different methods, where DCY and CH mean dried cellulose yarn and cellulose hydrogel; *CF* and *T* mean coagulation fraction and ring thickness, respectively.

Characterization	Sample	Quantifying parameter	Activation Energy (kJ/mol)
Microscopy	DCY	CF_{DCY}	69 ± 5
	CH	CF_{CH}	78 ± 4
	CH	T_H	71 ± 4

Interestingly, this value for mercerized cotton cellulose is lower than previously reported by this group for natural flax dissolution E_a of 98 ± 2 kJ/mol in [C2mim][OAc] (Hawkins et al., 2021) and natural cotton dissolution E_a of 96 ± 3 kJ/mol in [C2mim][OAc] (Liang et al., 2021). The values obtained are in broad agreement with previous activation energies from a range of techniques as described earlier in the introduction.

To understand the possible reasons for the different dissolution activation energies between the natural cotton reported in our previous

paper (Liang et al., 2021) and the mercerized one reported here, cellulose composition analysis and molecular weight measurement were conducted, and the results are tabulated in Tables S1 and S2. Compared with the natural cotton, the mercerized has less than half the number average molecular weight and the weight average molecular weight, and there is no measurable amount of hemicellulose detected in the mercerized cotton. Therefore, it is hypothesized that the processing history such as mercerization, which removes hemicellulose and decreases the molecular weight, potentially reduces the dissolution E_a of cellulose in [C2mim][OAc], and this is consistent with the findings reported by Qi et al.(Qi et al., 2008) but on NaOH/urea solvent system. A study of the effect of composition on the activation of cellulose-based materials is the focus of our current studies.

4. Conclusions

The dissolution kinetics of a mercerized cotton - based cellulose in [C2mim][OAc] has been studied at different dissolving times and temperatures. OM was used to characterize the morphology of both CH and DCY samples, and a ring-like coagulation region was found surrounding the central core. WAXD was applied to dried arrays for measuring their crystalline structure upon the dissolution, which shows that the raw material consists of cellulose I, cellulose II and amorphous cellulose, and a conversion from cellulose I to cellulose II and amorphous cellulose was found upon dissolution. The cellulose dissolution was found to follow TTS and an Arrhenius behaviour was found to describe the dissolution behaviour. For further understanding the dissolution behaviour, three quantifying methods based on OM results were used in different combinations of quantifying parameter and sample: CF_{DCY} for dried cotton yarns, CF_{CH} and T_H for cellulose hydrogels, and as a result, the activation energies are 69 ± 5 kJ/mol, 78 ± 4 kJ/mol and 71 ± 4 kJ/mol, respectively. These activation energies show an independence of sample and quantifying method, giving an average value of 73 ± 2 kJ/mol, which suggests that any parameter that quantifies dissolution can in principle be used to verify if TTS holds. The difference of dissolution E_a between the natural cotton cellulose (Liang et al., 2021) and the mercerized cotton cellulose in [C2mim][OAc], could be due to the mercerization reducing the molecular weight and changing the sample composition. This hypothesis could be further verified by mercerizing the natural cotton sample and comparing its dissolution E_a with the value reported in this paper.

In addition, the regional swelling ratio and water volume fraction were calculated based on the micrographs with a novel and straightforward method. It is more reliable than the widely reported gravimetric method (Saito et al., 2003) and more applicable on thin fibre-like samples. The findings such as the master curves in this paper can be used for fabricating all cellulose composites and the dissolution kinetics research of other fibre-like materials.

Funding

This research did not receive any specific grant from funding agencies in the public, commercial, or not-for-profit sectors.

CRediT authorship contribution statement

Yunhao Liang: Conceptualization, Methodology, Investigation, Writing – original draft, Visualization. **Michael E. Ries:** Supervision, Conceptualization, Writing – review & editing, Project administration. **Peter J. Hine:** Supervision, Conceptualization, Writing – review & editing, Project administration.

Declaration of competing interest

The authors declare that they have no known competing financial interests or personal relationships that could have appeared to influence the work reported in this paper.

Acknowledgements

The authors would like to thank Dr. Daniel L. Baker, Experimental Officer in the school of Physics and Astronomy, University of Leeds for the experiment training and instruction, and Prof. Antje Potthast, University of Natural Resources and Life Science for conducting decomposition measurement. Dr. James E. Hawkins, Xin Zhang and Maer Hael are also thanked for their contribution at discussions during the progress of this research. The data of this publication can be found at doi: https://doi.org/10.5518/1109.

Appendix A. Supplementary data

Supplementary data to this article can be found online at https://doi.org/10.1016/j.carbpol.2022.119541.

References

Budtova, T., & Navard, P. (2015). Viscosity-temperature dependence and activation energy of cellulose solutions. *Nord. Pulp Pap. Res. J., 30*(1), 99–104. https://doi.org/10.3183/npprj-2015-30-01-p099-104

Budtova, T., & Navard, P. (2016). Cellulose in NaOH–water based solvents: A review. *Cellulose, 23*(1), 5–55. https://doi.org/10.1007/s10570-015-0779-8

Cao, X., Peng, X., Sun, S., Zhong, L., Wang, S., Lu, F., & Sun, R. (2014). Impact of regeneration process on the crystalline structure and enzymatic hydrolysis of cellulose obtained from ionic liquid. *Carbohydrate Polymers, 111*, 400–403. https://doi.org/10.1016/j.carbpol.2014.05.004

Chang, C., Duan, B., Cai, J., & Zhang, L. (2010). Superabsorbent hydrogels based on cellulose for smart swelling and controllable delivery. *European Polymer Journal, 46*(1), 92–100. https://doi.org/10.1016/j.eurpolymj.2009.04.033

Chen, F., Sawada, D., Hummel, M., Sixta, H., & Budtova, T. (2020). Swelling and dissolution kinetics of natural and man-made cellulose fibers in solvent power tuned ionic liquid. *Cellulose, 27*(13), 7399–7415. https://doi.org/10.1007/s10570-020-03312-5, 5.

Cuissinat, C., & Navard, P. (2006a). Swelling and Dissolution of Cellulose Part 1: Free Floating Cotton and Wood Fibres in N-Methylmorpholine-N-oxide–Water Mixtures. *Macromolecular symposia, 244*(1), 1–18.

Cuissinat, C., & Navard, P. (2006b). Swelling and dissolution of cellulose part II: Free floating cotton and wood fibres in NaOH–water–additives systems. *Macromolecular Symposia, 244*(1), 19–30.

Cuissinat, C., & Navard, P. (2008). Swelling and dissolution of cellulose, part III: Plant fibres in aqueous systems. *Cellulose, 15*(1), 67–74.

Cuissinat, C., Navard, P., & Heinze, T. (2008a). Swelling and dissolution of cellulose, part V: Cellulose derivatives fibres in aqueous systems and ionic liquids. *Cellulose, 15*(1), 75–80.

Cuissinat, C., Navard, P., & Heinze, T. (2008b). Swelling and dissolution of cellulose. Part IV: Free floating cotton and wood fibres in ionic liquids. *Carbohydrate Polymers, 72*(4), 590–596. https://doi.org/10.1016/j.carbpol.2007.09.029

El Seoud, O. A., Koschella, A., Fidale, L. C., Dorn, S., & Heinze, T. (2007). Applications of ionic liquids in carbohydrate chemistry: A window of opportunities. *Biomacromolecules, 8*(9), 2629–2647. https://doi.org/10.1021/bm070062i

Gericke, M., Schlufter, K., Liebert, T., Heinze, T., & Budtova, T. (2009). Rheological properties of cellulose/ionic liquid solutions: From dilute to concentrated states. *Biomacromolecules, 10*(5), 1188–1194.

Glasser, W. G., Atalla, R. H., Blackwell, J., Malcolm Brown, R., Burchard, W., French, A. D., & Nishiyama, Y. (2012). About the structure of cellulose: Debating the Lindman hypothesis. *Cellulose, 19*(3), 589–598. https://doi.org/10.1007/s10570-012-9691-7

Hawkins, J. E., Liang, Y., Ries, M. E., & Hine, P. J. (2021). Time temperature superposition of the dissolution of cellulose fibres by the ionic liquid 1-ethyl-3-methylimidazolium acetate with cosolvent dimethyl sulfoxide. *Carbohydrate Polymer Technologies and Applications, 2*, Article 100021. https://doi.org/10.1016/j.carpta.2020.100021

Isogai, A., & Atalla, R. H. (1998). Dissolution of cellulose in aqueous NaOH solutions. *Cellulose, 5*(4), 309–319. https://doi.org/10.1023/A:1009272632367

Kabir, S. M. F., Sikdar, P. P., Haque, B., Bhuiyan, M. A. R., Ali, A., & Islam, M. N. (2018). Cellulose-based hydrogel materials: Chemistry, properties and their prospective applications. *Progress in Biomaterials, 7*(3), 153–174. https://doi.org/10.1007/s40204-018-0095-0

Le, K. A., Rudaz, C., & Budtova, T. (2014). Phase diagram, solubility limit and hydrodynamic properties of cellulose in binary solvents with ionic liquid. *Carbohydrate Polymers, 105*, 237–243. https://doi.org/10.1016/j.carbpol.2014.01.085

Liang, Y., Hawkins, J. E., Ries, M. E., & Hine, P. J. (2021). Dissolution of cotton by 1-ethyl-3-methylimidazolium acetate studied with time–temperature superposition for three different fibre arrangements. *Cellulose, 28*(2), 715–727.

Lindman, B., Karlström, G., & Stigsson, L. (2010). On the mechanism of dissolution of cellulose. *Journal of Molecular Liquids, 156*(1), 76–81. https://doi.org/10.1016/j.molliq.2010.04.016

Lynd, L. R., Weimer, P. J., Van Zyl, W. H., & Pretorius, I. S. (2002). Microbial cellulose utilization: Fundamentals and biotechnology. *Microbiology and Molecular Biology Reviews, 66*(3), 506–577.

Mahmood, H., Moniruzzaman, M., Yusup, S., & Welton, T. (2017). Ionic liquids assisted processing of renewable resources for the fabrication of biodegradable composite materials. *Green Chemistry, 19*(9), 2051–2075. https://doi.org/10.1039/c7gc00318h

McCormick, C. L., Callais, P. A., & Hutchinson, B. H., Jr. (1985). Solution studies of cellulose in lithium chloride and NN-dimethylacetamide. *Macromolecules, 18*(12), 2394–2401.

Plechkova, N. V., & Seddon, K. R. (2008). Applications of ionic liquids in the chemical industry. *Chemical Society Reviews, 37*(1), 123–150.

Qi, H., Chang, C., & Zhang, L. (2008). Effects of temperature and molecular weight on dissolution of cellulose in NaOH/urea aqueous solution. *Cellulose, 15*(6), 779–787.

Quintana, R., Persenaire, O., Bonnaud, L., & Dubois, P. (2012). Recent advances in (reactive) melt processing of cellulose acetate and related biodegradable bio-compositions. *Polymer Chemistry, 3*(3), 591–595. https://doi.org/10.1039/C1PY00421B

Ries, M. E., Radhi, A., Keating, A. S., Parker, O., & Budtova, T. (2014). Diffusion of 1-ethyl-3-methyl-imidazolium acetate in glucose, cellobiose, and cellulose solutions. *Biomacromolecules, 15*(2), 609–617. https://doi.org/10.1021/bm401652c

Saito, H., Sakurai, A., Sakakibara, M., & Saga, H. (2003). Preparation and properties of transparent cellulose hydrogels. *Journal of Applied Polymer Science, 90*(11), 3020–3025. https://doi.org/10.1002/app.13015

Sen, S., Martin, J. D., & Argyropoulos, D. S. (2013). Review of cellulose non-derivatizing solvent interactions with emphasis on activity in inorganic molten salt hydrates. *ACS Sustainable Chemistry & Engineering, 1*(8), 858–870. https://doi.org/10.1021/sc400085a

Swatloski, R. P., Spear, S. K., Holbrey, J. D., & Rogers, R. D. (2002). Dissolution of cellulose with ionic liquids. *Journal of the American Chemical Society, 124*(18), 4974–4975. https://doi.org/10.1021/ja025790m

Walden, P. (1914). Ueber die Molekulargrösse und elektrische Leitfähigkeit einiger geschmolzenen salze. *Известия Российской академии наук. Серия математическая, 8*(6), 405–422.

Yue, Y., Zhou, C., French, A. D., Xia, G., Han, G., Wang, Q., & Wu, Q. (2012). Comparative properties of cellulose nano-crystals from native and mercerized cotton fibers. *Cellulose, 19*(4), 1173–1187. https://doi.org/10.1007/s10570-012-9714-4

Zhang, X., Liu, X., Zheng, W., & Zhu, J. (2012). Regenerated cellulose/graphene nanocomposite films prepared in DMAC/LiCl solution. *Carbohydrate Polymers, 88*(1), 26–30. https://doi.org/10.1016/j.carbpol.2011.11.054

Zhang, X., Ries, M. E., & Hine, P. J. (2021). Time-temperature superposition of the dissolution of silk fibers in the ionic liquid 1-ethyl-3-methylimidazolium acetate. *Biomacromolecules, 22*(3), 1091–1101. https://doi.org/10.1021/acs.biomac.0c01467

Zhao, H., Kwak, J. H., Wang, Y., Franz, J. A., White, J. M., & Holladay, J. E. (2007). Interactions between cellulose and N-methylmorpholine-N-oxide. *Carbohydrate Polymers, 67*(1), 97–103. https://doi.org/10.1016/j.carbpol.2006.04.019